Journal of the Meteorological Society of Japan, Vol. 77, No. 3, pp. 753–769, 1999

10–25 day Intraseasonal Variations of Convection and Circulation over East Asia and Western North Pacific during Early Summer

By Yoshiki Fukutomi and Tetsuzo Yasunari

Institute of Geoscience, University of Tsukuba, Tsukuba, Japan

(Manuscript received 7 May 1998, in revised form 29 March 1999)

Abstract

The space-time evolution of intraseasonal convection and circulation anomalies in the 10–25-day period range over East Asia and western North-Pacific Monsoon regions are explored for four early summer seasons from 1991 to 1994. The paper primarily focuses on the linkage between tropical convection over the South China Sea, and lower-tropospheric circulation over the East Asian subtropics on this time scale. The composite results show that quasi-periodic fluctuations of convection on the 10–25-day time scale over the South China Sea, are associated with large-scale circulation in the Asian-Pacific region. The development of subtropical circulation and convection takes place through changes in large-scale circulation on this time scale.

10–25-day enhanced (suppressed) convection occurs in conjunction with well-organized cyclonic (anti-cyclonic) circulation anomalies over the South China Sea. A downstream wave train extending from the South China Sea into the North Pacific, is built up in the lower troposphere associated with this convective activity. This wave train is probably interpreted as a Rossby mode response to the anomalous heating (cooling). Following the peak of enhanced convection, the East Asian subtropical anomalous anti-cyclone maintains its strength as part of this wave train, and couples with enhanced subtropical convection along the northern flank of this anti-cyclonic cell. This development of convection in the subtropical frontal zone is due to an increase in the low-level westerlies at the northern flank of this anti-cyclonic circulation. In addition, this subtropical anomalous anti-cyclone moves southwestward from the subtropics into the South China Sea region, and appears to initiate subsequent suppressed convection. In contrast, the southwestward migration of subtropical cyclonic anomalies also occurs following the inactive convection over the South China Sea, and this behavior appears to trigger the subsequent active convection over this region. These features suggest that mutual interactions between the tropics and the subtropics on this time scale play important roles on the variability of monsoon convection and circulation over East Asia, and western North Pacific.

In the upper level strongest divergent outflow (convergent inflow) occurs in the convective (non-convective) region and the significant wave train is maximally intensified in the mid-latitude at the convective peak. Upper-level circulation also appears to be forced by heating (cooling) located over the South China Sea region. These circulation features confirm that 10–25-day variations of convection over the South China Sea are one of the effective forcings for the large-scale circulation during the early summer season.

1. Introduction

During the past two decades or so, numerous studies have documented the various aspects of the intraseasonal oscillations of convection and circulation in the Asian monsoon region. Since high-quality global objective analysis data sets have been available after the 1979 FGGE (First GARP [Global Atmospheric Research Program] Global Experiment)/MONEX (Monsoon Experiment) year, many investigators have focused on relationships between the equatorial eastward propagating 30–60-day convective oscillations, which is the so-called Madden-Julian Oscillation (MJO) discovered by Madden and Julian (1971, 1972) and the monsoon circulation systems. These previous studies have shown that the MJO is coupled with the northward propagating trough/ridge system which appears as activities of the Asian summer monsoon (*e.g.*, Yasunari, 1981; Krishnamurti and Subrahmanyam, 1982; T. Murakami *et al.*, 1984a, b; Lau and Chan, 1986; Chen and M. Murakami, 1988; Chen and Chen, 1993a).

Corresponding author: Tetsuzo Yasunari, Institute of Geoscience, University of Tsukuba, Ibaraki 305-8571, Japan. E-mail: yasunari@atm.geo.tsukuba.ac.jp

On the other hand, the intraseasonal oscillations in 10–20-day period range have also been noticed in the Indian monsoon region by M. Murakami (1976), Yasunari (1979), Krishnamurti and Ardanuy (1980), Krishnamurti and Bhalme (1976), and Chen and Chen (1993b). Though most of these studies have found some common features of the 10–20-day mode in this region, a more generalized view of this mode with the data of many summer seasons has not been well investigated yet.

Comparatively fewer studies have documented variations on this shorter intraseasonal time scale in the East Asian summer monsoon (EAM) (Lau, 1992), and western North-Pacific monsoon (WNPM) (T. Murakami and Matsumoto, 1994) region. Analyzing the seasonal and the intraseasonal variability associated with the EAM, Lau *et al.* (1988) found a 20-day oscillation of the precipitation during the Mei-yu regime. A recent study by Chen and Chen (1995) noted the effect of the 12–24-day mode on the onset and break of the South China Sea monsoon for the summer MONEX period. Lau and Yang (1996) found the rainfall oscillations, with a distinct time scale of about 15–20 days, in the Indo-China and East Asian region. These oscillations become prominent after the sudden jump of the ITCZ (Inter Tropical Convergence Zone) from the equator to 10°–20°N, which corresponds to the onset of monsoon convection in mid-May to early-June.

Although variations in the 10–20-day band have been found in those previous studies, an accurate description of the role of tropical convection on this time scale, in affecting the circulation over the EAM and WNPM region during summer has been limited. A question may arise how tropical convection on this time scale affects large-scale circulation. Of particular interest is the linkage of convective activity in the South China Sea region with the subtropical frontal zone called the Baiu frontal zone (BFZ) during the early summer season. In general, the primary contribution of tropics for the formation of the BFZ is the supply of moisture by low-level poleward flow along the periphery of the Pacific subtropical anti-cyclone (*e.g.*, Ninomiya and Muraki, 1986; Kato, 1989; Kodama, 1992, 1993). However, substantial roles of the 10–20-day mode in the circulation change in the BFZ region have not been well understood. As will be shown later, this short-term intraseasonal variability seems to be one of the important components for tropical-extratropical interactions in the various space and time scale, as well as the MJO time scale variations during the early summer season.

We will focus on the space-time evolution of convection and circulation anomalies on the 10–25-day intraseasonal time scale in the EAM and WNPM region. This slight broader band based on the spectral results is selected in this study. We will examine the composite relationships between tropical convection, and large-scale circulation changes on this time scale in the early summer season from June through July, particularly relevant to the EAM of 1991–94. This period almost corresponds with the Baiu season (Ninomiya and Akiyama, 1992). An emphasis is laid on convective activities over the South China Sea, and the corresponding subtropical circulation and convection. The possible processes responsible for subsequent development of lower-tropospheric subtropical westerlies and convection are presented. In addition, upper-level circulation changes associated with convective activity are also described. In Section 2, we describe the data and method used for the present analysis. In Section 3, the mean convection and circulation features during the early summer season are shown. The results of time series analysis of OLR anomalies are presented in Section 4. The propagation properties are also stated in this section. Composite relationships between 10–25-day convection over the South China Sea, and large-scale circulation anomalies, are presented in Section 5. The possible dynamics of the convection and circulation systems are discussed in Section 6.

2. Data and methodology

The primary datasets used in this study are the ECMWF/TOGA basic level III global analyses obtained from the National Center for Atmospheric Research (NCAR), and the outgoing longwave radiation (OLR) dataset produced by NOAA/CDC (Climate Diagnostics Center). The ECMWF archive contains six meteorological variables for every 12 hours (0000 and 1200 UTC) on a 2.5°×2.5° grid at 12 pressure levels. We extracted the horizontal wind at 200 and 850 hPa from this dataset. The twice-daily data at 0000 and 1200 UTC are averaged to form the daily mean data. The stream functions were computed from the wind data using the spectral transform method by the spherical harmonic truncation at R25.

In the present analysis, we used the datasets of the four northern summers (May–September) of 1991–94. For all variables, seasonal trend of each summer was removed prior to the time series analysis, by subtracting the quadratic trend at each grid point. The seasonal mean of each summer was also removed from daily time series. We applied the spectral analysis by the fast Fourier transform (FFT) method to all the anomalies thus obtained to investigate the prominent period range of fluctuations in selected locations. Butterworth band-pass filter (Kaylor, 1977) was applied to the time series of each anomaly in order to examine the intraseasonal fluctuations of the large-scale circulation and convection. Hsu and Lin (1992) applied this filtering procedure, and they successfully removed the high-frequency variability to investigate the low-frequency teleconnection pat-

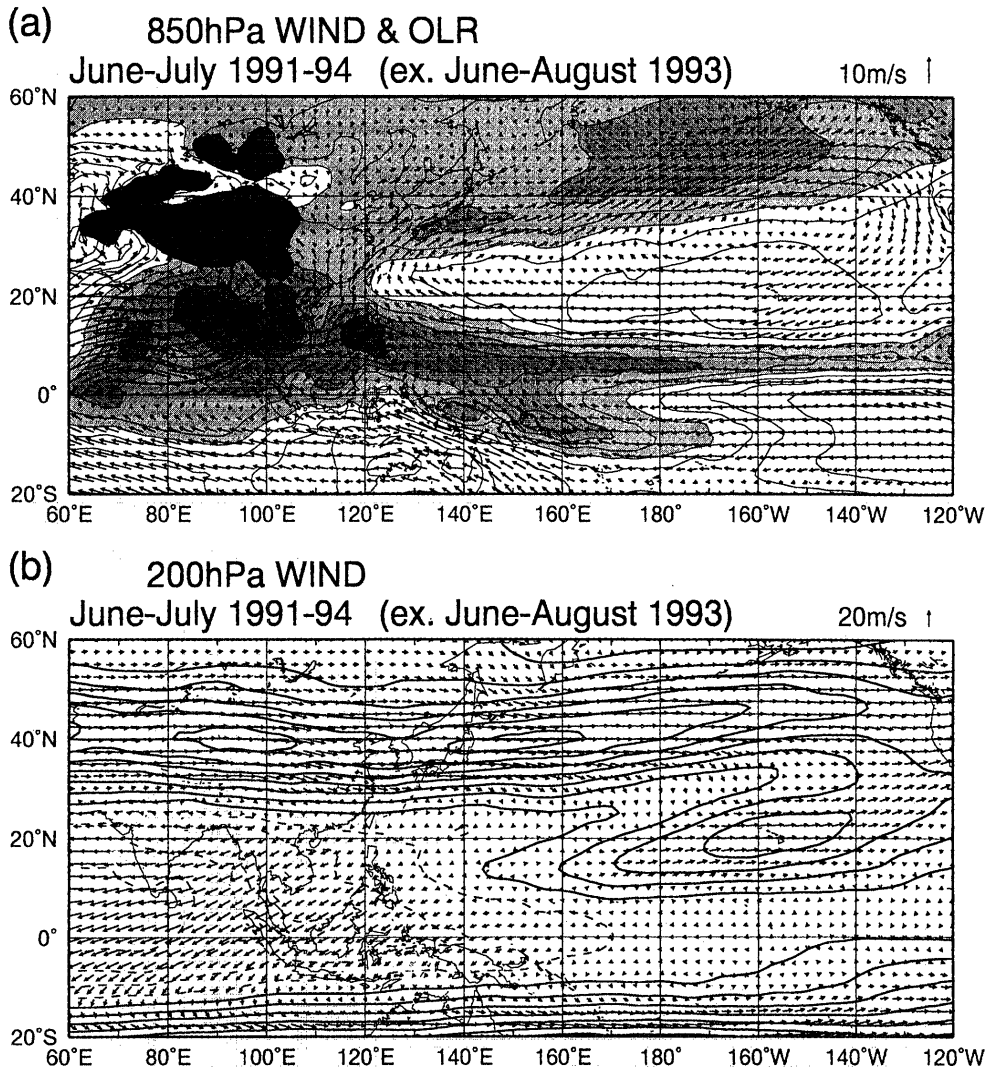

Fig. 1. Distributions of mean fields during the early summer season (June–July) for 1991–1994. The June–August period is employed exceptionally for 1993. (a) OLR and 850-hPa wind field. Contour interval is 10 W m^{-2}. The regions of OLR values less than 240 W m^{-2} are shaded. (b) 200-hPa wind field and isotaches of zonal wind. Contour interval is 10 m s^{-1}, with zero contour omitted. Negative contours are dashed.

terns on the intraseasonal time scales. The composite technique was also applied in order to examine the structure of convection and circulation on this intraseasonal time scale. Details of this technique are described in Section 5.

3. Large-scale mean conditions

In this section we describe the large-scale mean circulation and convective activities during the early summer season (see Fig. 1) since we intend to examine the intraseasonal variations during the period when the BFZ is prominent. For this purpose, we employ the June–July period to describe the basic feature of this season. However in the summer of 1993, the activities of subtropical front in East Asia did not disappear even after late-July and persisted for abnormally long period (Kodama, 1997), and prominent convection zone was maintained in the subtropics by mid-August. Therefore a notable interaction between the tropics and the subtropical frontal systems may have occurred even after late-July. For this reason, the June–August period was employed as the early summer season exceptionally in 1993.

Figure 1a shows the four years composites of OLR and 850-hPa wind fields in June–July (June–August in 1993), which represents the mature stage of the Indian monsoon and the Baiu. ITCZ extends from the Bay of Bengal to the Philippines, located at 5°–15°N with enhanced convection over these regions. The wind speed of the monsoon westerlies from the Arabian Sea increases in May (not shown), and these westerlies converges the South China Sea. The confluence zone from the westerly and the easterly is re-

markably seen over the Philippine Islands. The BFZ in East Asia is established with a zonally stretched structure along the northern periphery of the Pacifc subtropical high.

The upper-level circulation pattern at 200-hPa level averaged through the same period as Fig. 1a is shown in Fig. 1b. Anti-cyclonic circulation centered to the south of Tibetan plateau (*i.e.*, Tibetan high) emerges. Cross-equatorial northeasterly flow is established over entire tropical monsoon region. We can also see that the axis of mid-latitude Asia and Pacific jet lies around 40°N. These characteristics are accompanying the Indian monsoon onset as documented by many previous studies.

4. Statistical analyses and temporal characteristics

We apply some statistical analyses to the detrended OLR anomalies to demonstrate the basic characteristics of 10–25-day signals before the composite analysis. We also intend to detect the remarkable convection events for the composite analysis that will be applied in the next section.

4.1 Power spectrum of OLR

A spectral analysis was performed to the daily OLR anomalies at selected grid points in order to determine the optimal filtering band for later analyses. We chose time series at 17.5°N, 115°E from May to September 1991–94, which is the location of the total variance maximum in the WNPM region. The red-noise spectrum and its corresponding 95% confidence level obtained from a first-order red noise model (Gilman *et al.*, 1963; Mitchell, 1966) are also shown. Ko and Vincent (1995, 1996) used these methods of estimation of power spectral density and the significance test, and they could detect the signal on shorter (5–20-day) intraseasonal timescales.

A significant spectral peak at 18 days in four years ensemble power spectrum is found in Fig. 2. This peak that exceeds the 95% confidence curve is centered on the distinct 10–25-day range. Another peak in periods greater than 30 days associated with the MJO convection is also found here. These characteristics indicate that the South China Sea region is important for the growth of MJO time scale convection, as cited by many previous investigations. On the whole, the existence of the prominent 10–25-day oscillations of convection is one of the important parts of the variation of the ITCZ. The example of spectra given here is similar to that by Chen and Chen (1995).

4.2 Spatial distribution of OLR variability

Figure 3 presents the geographical distribution of the variance of OLR for the 10–25-day band, and its percentage to total variance over the entire Asian monsoon region. Figure 3a gives the variance for the 10–25-day period range for the early summer

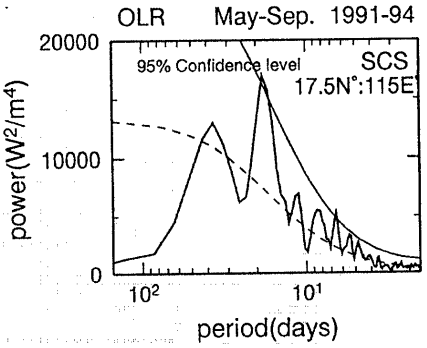

Fig. 2. Ensemble power spectrum of May to September 1991–94 OLR daily time series (153 days) for the point 17.5°N, 115°E. Red noise spectrum (dotted curve) and its 95 % confidence level (solid curve) are also shown.

seasons of 1991–94 stated in Section 3. The variance is ensemble average of individual seasons. It is apparent that the region of highest power exists over the South China Sea where the strong signal of the 10–25-day period range is found in the spectral result (Fig. 2). It is interesting to note that a large power greater than 400 W^2 m^{-4} is partly seen in the BFZ region. In the lower panel (Fig. 3b), a high percentage greater than 30 percent of the total variance covers the South China Sea. The characteristics mentioned above indicate that the South China Sea region is the center of action of OLR fluctuations of this time scale during this season, and that is an appropriate base region to investigate the coherent fluctuations of circulation with this convective signal.

4.3 Time sequences of convective activity in the base region

The detrended daily OLR anomalies (thin line), and the corresponding anomalies based on 10–25-day filtered values (thick line) over the South China Sea in an area 110°–120°E, 10°–20°N, are depicted in Fig. 4. It can be seen that the quasi-periodic oscillations of convection on this time scale became active from the beginning of June in 1991, 92, 94. In 1993, this signal became prominent from late-June, and most active events appear in July through mid-August. Black dots in each figure represent the peak phases of active convection events on the 10–25-day timescale, with the peak values of less than −1.0 standard deviation (−18.4 W m^{-2}) during the early summer season. We perform the composite analysis in the following section with reference to these filtered anomalies and selected convection events.

4.4 Propagation characteristics

The examples of the propagation properties of 10–25-day filtered OLR and zonal wind anomalies, are given in the composite longitude-time diagrams of

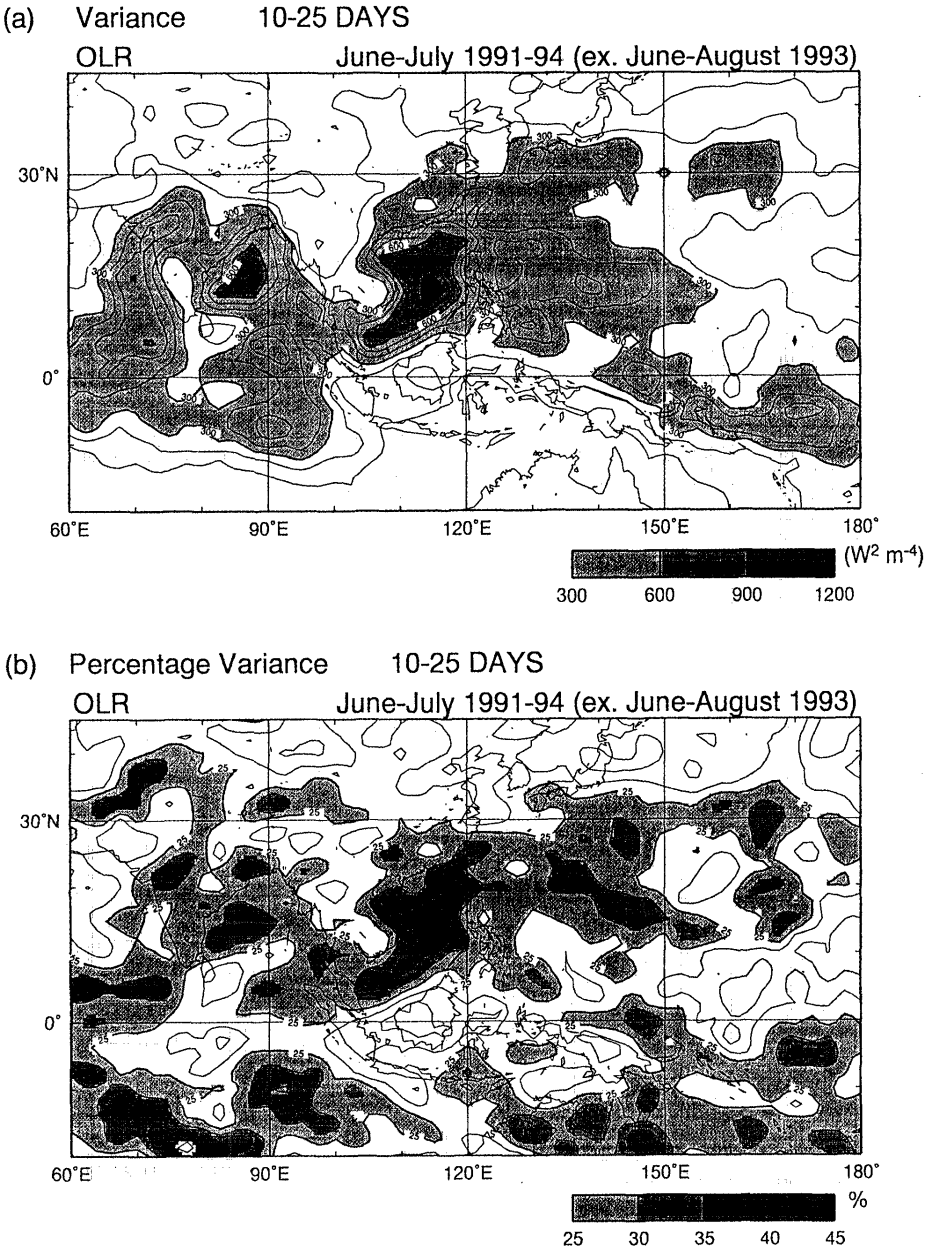

Fig. 3. (a) Variance of OLR in the 10–25-day band for the same period as Fig. 1. (b) Percentage of total variance in the same band for the same period as (a). Contour interval is 100 W^2 m^{-4} in Fig. 3a, 5 % in Fig. 3b. Shading denotes values less than 300 W^2 m^{-4} in Fig. 3a, less than 25 % in Fig. 3b.

OLR and zonal wind anomalies illustrated in Fig. 5. It is a well-known feature that these short-term intraseasonal oscillations occur in the form of westward propagations over the tropical monsoon region (*e.g.*, Nakazawa, 1986; Chen and Chen, 1993b, 1995). We have also confirmed this marked characteristic in the South China Sea region. These cross-sections are constructed based on the time series of OLR anomalies in Fig. 4. Day 0 is corresponding to the enhanced convective peak selected in the previous subsection. Averaged phase speed of −7.6 m s^{-1} westward are estimated in this diagram. This westward phase speed is faster than that of the 20–70-day range at about −5 m s^{-1} along 15°N as noted by Wang and Xie (1997).

5. Space-time evolution of convection and circulation anomalies

In the previous section, some prominent features of convective signals were seen from the time series analysis. To better understand the relationships between 10–25-day convection over the South China Sea and the large-scale circulation anomalies, daily OLR and wind anomalies at 850- and 200-hPa levels

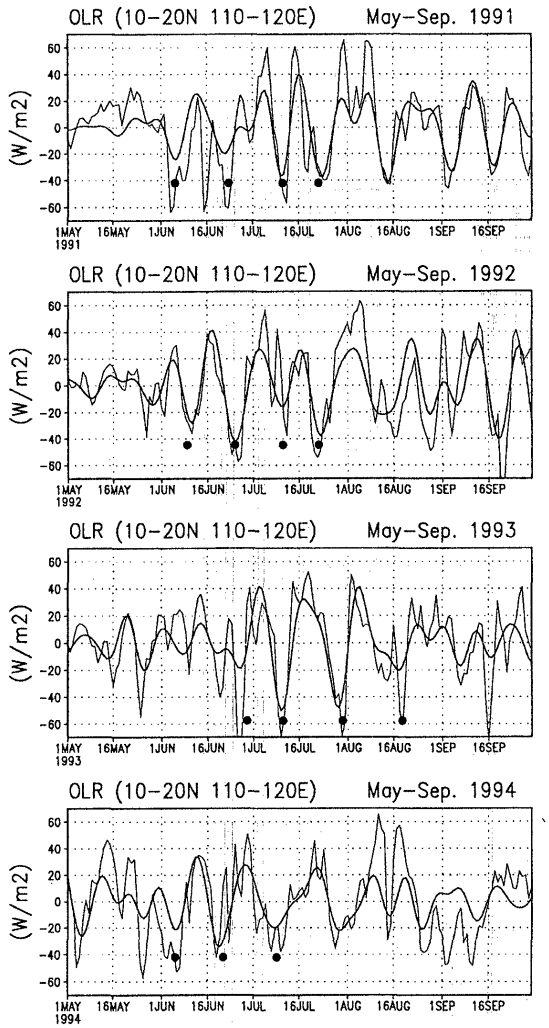

Fig. 4. Time series of OLR anomalies (thin line) and 10–25-day filtered anomalies (thick line) avereged over 10°–20°N, 110°–120°E in individual summers. The black dots represent the selected active convection events for the composite analysis.

are examined through the composite analysis in this section.

5.1 Composite procedure

The space-time evolution of variables associated with tropical convective activity will be described using the composite anomalies constructed on the basis of filtered time series shown in Fig. 4. We divide complete cycles of filtered OLR anomalies, which include convection events previously selected into the eight categories (phases). A total of 15 cycles during the early summer season were selected for the composting technique. This composite variation of convection index is given in Fig. 6. Category 3 is assigned to the phase when the OLR anomaly becomes minimum, while Category 7 is assigned to the phase when the OLR anomaly becomes maximum. These categories correspond to the active phase and the inactive phase of the convection. The composite value of OLR anomaly at negative (positive) peak is about −30 (30) W m^{-2}. These values correspond to about −1.6 (1.6) standard deviation in this base region. Category 1 is the transition phase from the maximum to the minimum, and Category 5 is denoted as the opposite situation to Category 1. Category 2, 4, 6 and 8 are assigned to the intermediate phases. Composite maps for OLR and any other variables were made referring to these categories, in order to examine the behavior of convection and circulation anomalies. The statistical local significance at 95 % level of each composite map was tested by the same method described in T. Murakami (1987).

5.2 The evolution of OLR and lower circulation anomalies

Figure 7 represents successive composite maps of OLR and circulation anomalies of the 10–25-day component from Category 1 to 8. The OLR negative (positive) anomalies less (greater) than −5 (5) W m^{-2} are darkly (lightly) shaded. The vectors where either u or v component surpasses the 95 % local confidence level according to a standard t-test are plotted. The stream function anomalies are drawn in an entire region.

At Category 1 westerly anomalies appear in the southern portion of the South China Sea and the western Pacific prior to the development of convective signal. An anti-cyclonic circulation is decaying over the Indo-China peninsula. A cyclonic circulation is located in the subtropical region in the western North-Pacific.

During the period from Categories 1 to 3, a cyclonic circulation in the subtropics moves southwestward and westerly anomalies also move westward into the South China Sea. Negative OLR anomalies develop and cover the South China Sea region rapidly. In Category 3, this OLR signal reaches its minimum, which is exactly the peak of enhanced convection. A cyclonic disturbance develops in conjunction with enhanced convection at this stage. Concurrently a wave train is built up from the South China Sea to the North Pacific. An anti-cyclonic circulation centered at 30°N, 135°E in the subtropics emerges as part of this wave train. Anomalous northeasterly flow as southeastern part of this subtropical anti-cyclonic cell is clearly seen. These transient wind anomalies imply a decrease of westerlies in the variation of the total wind field. Positive OLR anomalies cover the subtropical region along 20°–30°N, indicating that anomalous convection is suppressed in this region.

At Category 4, which is the phase just after the convective peak, a cyclonic circulation moves westward to the Indo-China peninsula and weakens be-

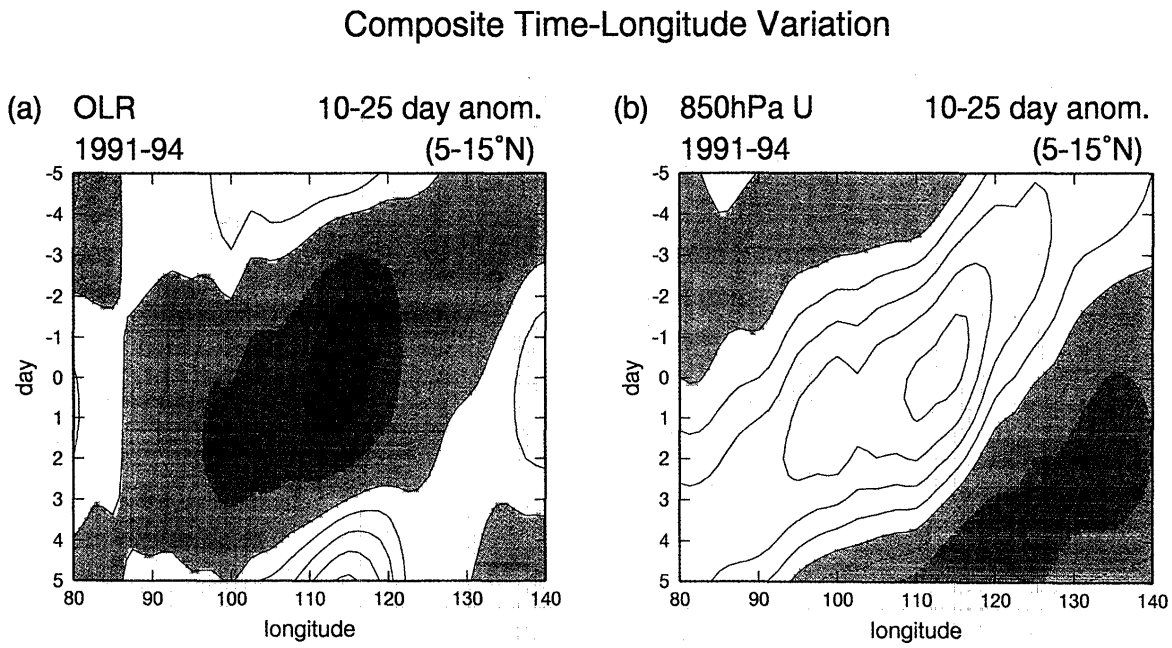

Fig. 5. Composite longitude-time diagram along 5°–15°N of 10–25-day band-pass filtered anomalies. (a) OLR anomalies. Contour interval is 5 W m^{-2} with negative anomalies are shaded. (b) Zonal wind anomalies. Contour interval is 0.5 m s^{-1} with negative anomalies are shaded.

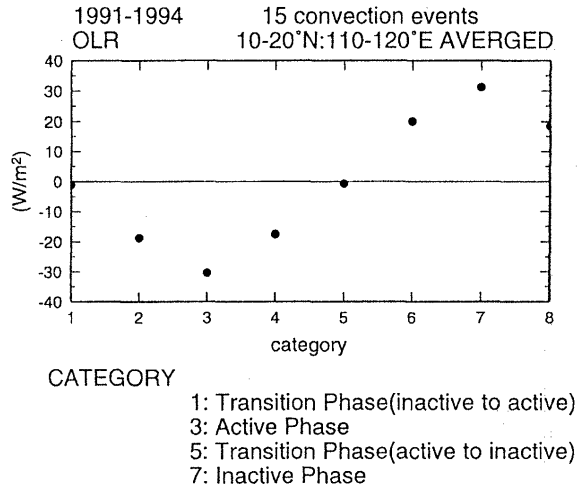

Fig. 6. Composite variations of the 10–25-day filtered OLR anomalies avereged over the same area as in Fig. 4.

cause of decaying convection. Anomalous westerlies extend westward from the South China Sea to the Arabian Sea. This feature implies that the monsoon westerly flow is accelerated in these regions. On the other hand an anti-cyclonic circulation in the subtropics is more intensified than in Category 3. It is also worth noting that significant easterly anomalies are found in the tropical western Pacific to the southeast of Philippines.

We next examine the phases following convective maximum over the South China Sea (through Category 5 to 8). From Category 5 to 6, a cyclonic disturbance over the South China Sea–Indo-China peninsula weakens further and disappears. The spreading of positive OLR anomalies results in suppressed convection over the South China Sea and Philippines. Easterly wind anomalies propagate westward from the east of Philippines into the South China Sea along 5°–10°N. While in the subtropical region, an anti-cyclonic circulation maintains its strength and is migrating southwestward into the South China Sea. Westerly wind and negative OLR anomalies start developing at the northern flank of this anti-cyclonic cell. The negative OLR anomalies become more zonally elongated and shift southward coupled with this migrating anti-cyclone. This OLR signal reveals that anomalous convection is enhanced in the BFZ region around 110°–140°E.

In Category 7, the pattern of OLR and circulation anomalies is reversed as compared to that in Category 3. Suppressed convection and an anomalous anti-cyclonic circulation can be seen over the South China Sea region. Southwestward migration of this anti-cyclonic circulation during Category 4 through 7 appears to initiate suppressed convection in this region. An out of phase wave train pattern as compared to Category 3 extends from the South China Sea to the North Pacific. A cyclonic circulation, which is part of this wave train, emerges in the BFZ region. Anomalous enhanced convection around 30°N is co-located with this anomalous

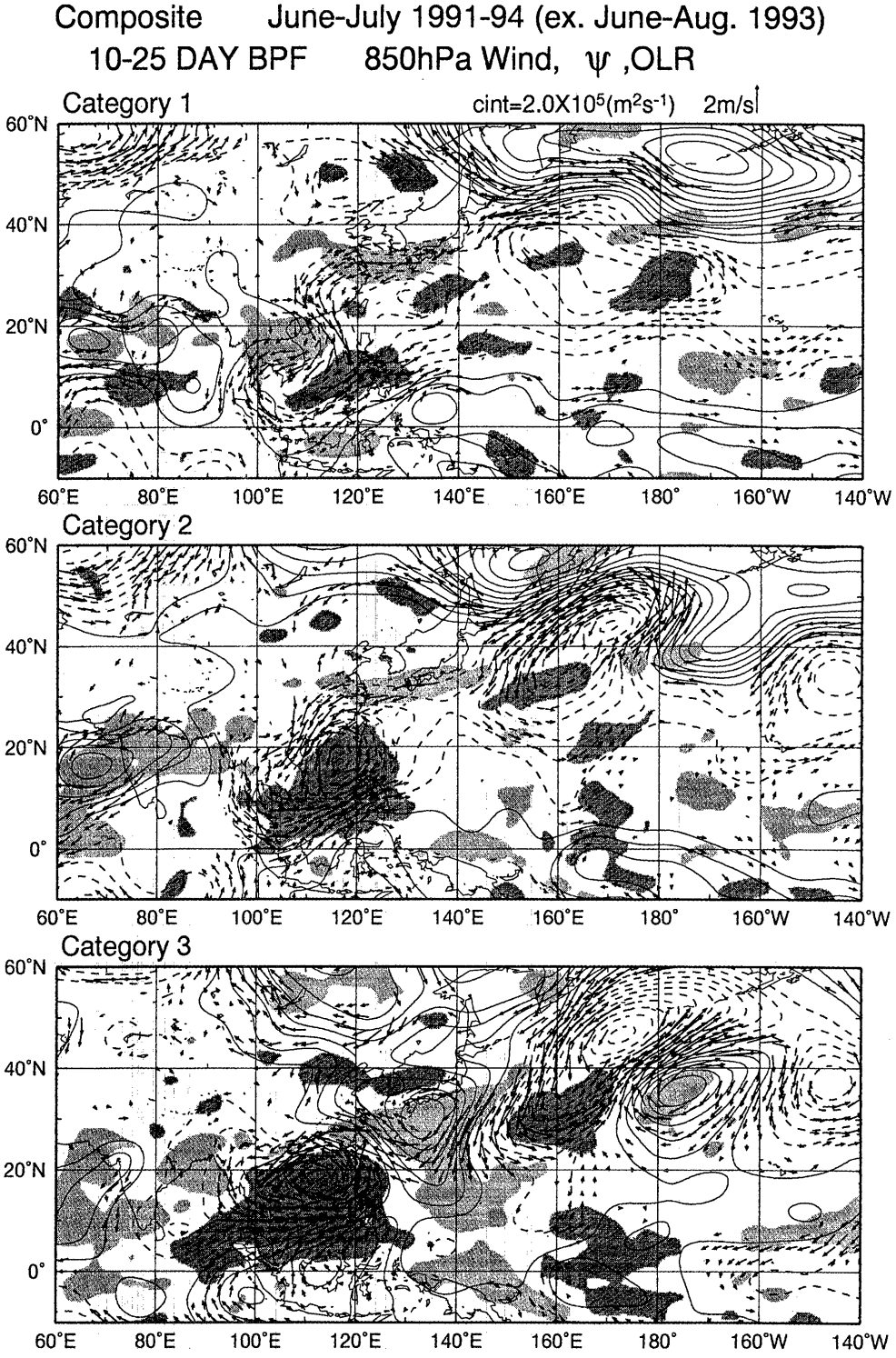

Fig. 7. Spatial distribution of composite OLR, 850-hPa stream function and vector wind anomalies in the 10–25-band from Category 1 through Category 8. Contour interval is 3.0×10^5 m^2 s^{-1}. OLR anomalies less (greater) than -5 (5) W m^{-2} are darkly (lightly) shaded. Only locally statistically significant wind vectors are shown.

trough. This zonally oriented subtropical convective band is coupled with subtropical westerly anomalies as southern flank of this anomalous trough.

From Category 7 through 8, intensified easterly anomalies blow up from the east of the Philippines to the Bay of Bengal. This signal decelerates the monsoon westerlies in the total wind field. An anomalous ridge is apparently seen over the Bay of

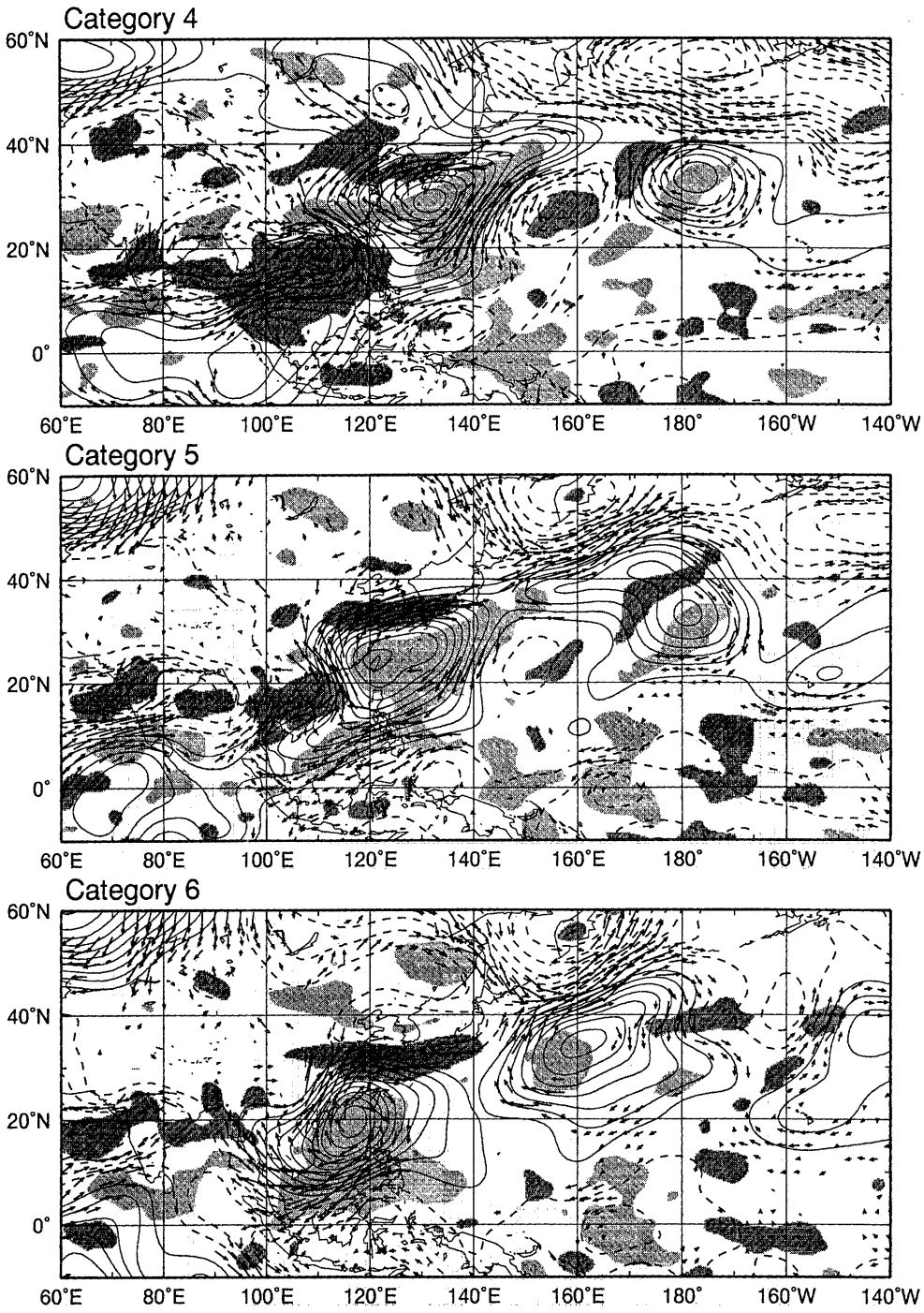

Fig. 7. (Continued)

Bengal and Indo-China Peninsula, which may correspond with the break condition over these regions. A southwestward migration of a cyclonic circulation from the subtropics into the South China Sea from Category 8 to 2 seems to trigger the next convective disturbance in the South China Sea region.

From this time sequence, it is apparently seen that the low-level circulation anomalies associated with 10–25-day convection have an well-organized structure. The life cycle of a cyclonic (anti-cyclonic) circulation accompanied by enhanced (suppressed) convection is clearly seen in the South China Sea region. Significant wind anomalies appear also in the subtropical frontal zone. This is due to the generation of an anti-cyclonic (cyclonic) circulation that is part of the wave train arching into the North Pacific. This pattern is probably regarded as a Rossby wave response to tropical heating over the South China Sea. This wave train nature is similar to the MJO-scale Rossby wave emanation from the

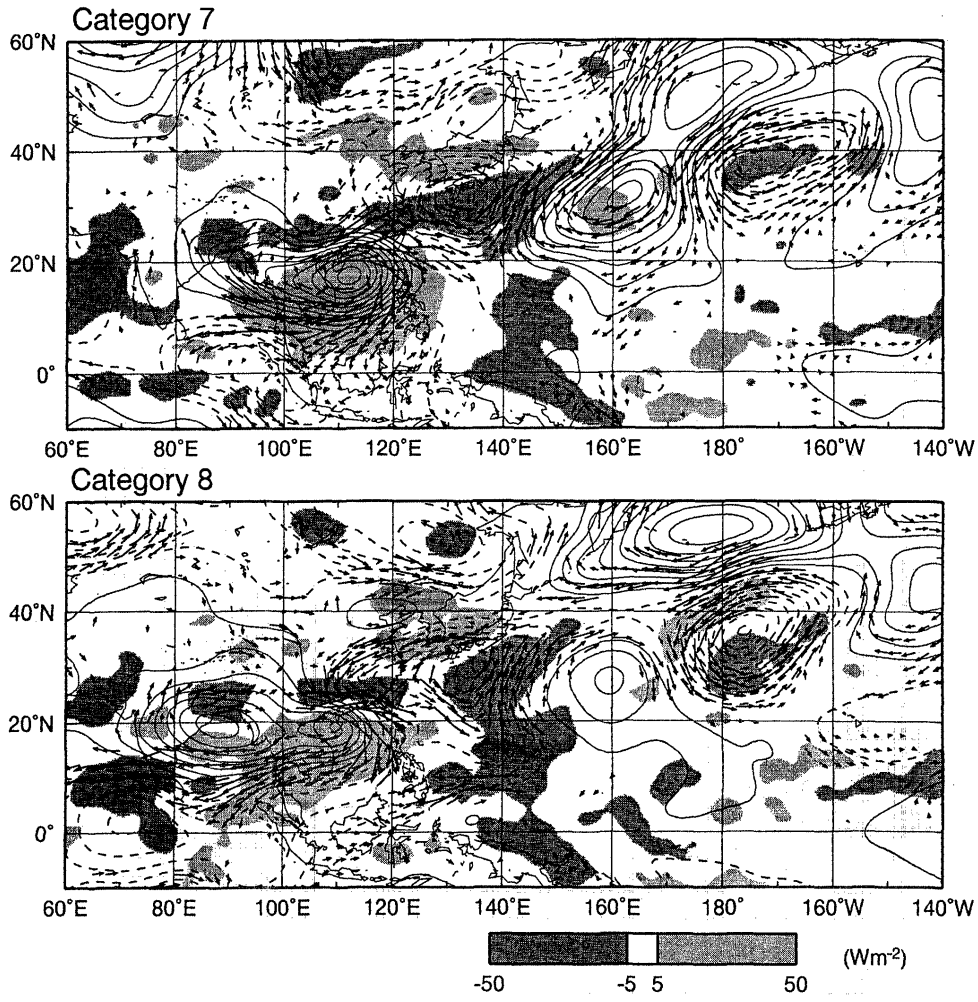

Fig. 7. (Continued)

WNPM region to mid-latitude during an entire summer season indicated by Kawamura *et al.* (1996). The present composite wave patterns in Fig. 8 have almost wavenumber 6 scale. The sizes of anomalous cells in Fig. 8 seem to be smaller than in the MJO case.

Development of subtropical wind anomalies may affect the contemporaneous OLR fluctuations in the BFZ region. Especially during Category 4 to 7, the enhanced convective area having zonally elongated shape is coupled with the westerly anomalies at the northern flank of anti-cyclonic cell. This subtropical convection may be reinforced by moisture transport, and its convergence associated with the maintenance of this anti-cyclonic circulation.

In order to clarify this point, we examine the moisture field in the lower troposphere. Figure 8 shows the composite fields in the moisture fluxes by the 10–25-day component and its convergence at 850-hPa level. Here the zonal component of the 10–25-day filtered moisture flux can be written as $\widehat{qu}$ where u is the zonal component wind, q is the specific humidity, a hat indicates the 10–25-day filtered transients. Meridional component is also estimated in the same manner. The time sequence of composite moisture field from Category 5 through 7 is presented here. The pattern of these vector fields is very similar to the composite wind fields given in Fig. 7. The local westerly moisture flow is evident over the subtropics in association with the southwestward migrating anti-cyclonic circulation. In addition the convergence area extends around 30°N from Category 5 to 7. In the specific humidity ($\hat{q}$) field (Fig. 9), significant anomalous moisture band develops in the BFZ region with eastward progression. This feature suggests that moist air accumulates in the subtropical region during this period. These features overlapped with the subtropical convective band (Fig. 7) suggest that local increase of moisture transport contributes to the enhancement of subtropical convection.

It should be noted from the aforementioned characteristics that tropical convection on the 10–25-day timescale could have significant impact on the low-

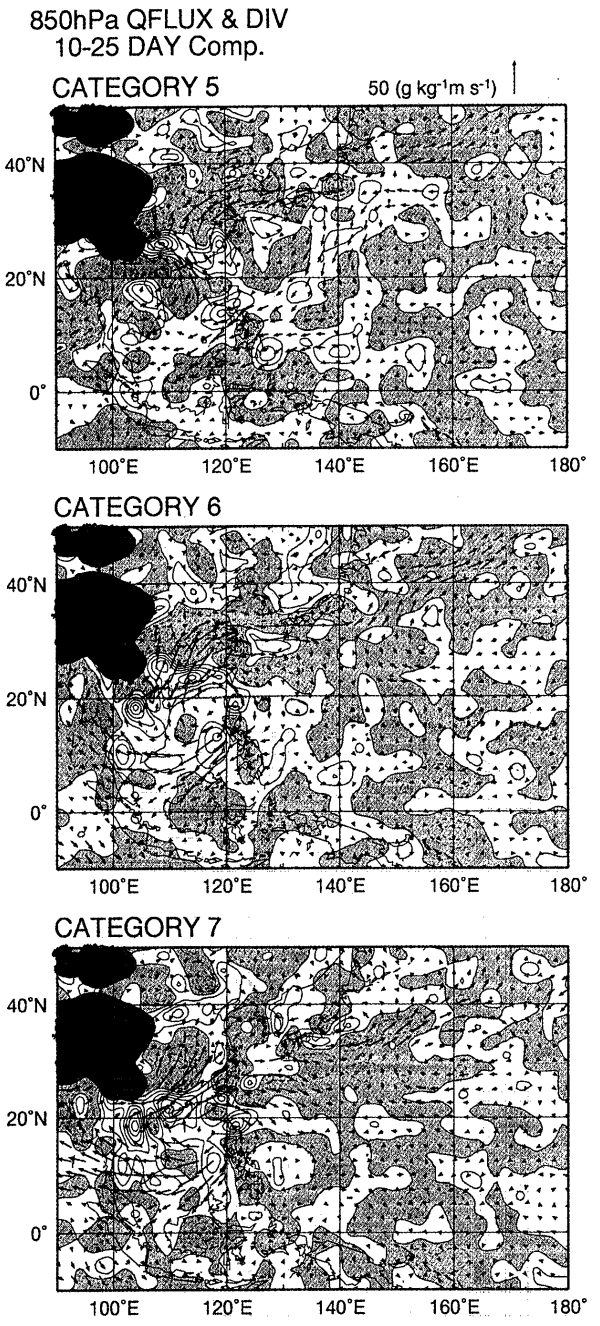

Fig. 8. Composite moisture flux vectors ($g\ kg^{-1}\ m\ s^{-1}$) of the 10–25-day component and its divergence from Category 5 through 7 at 850 hPa. Negative (converegent) regions are shaded. Contour interval is $2\times10^{-6}\ g\ kg^{-1}\ s^{-1}$.

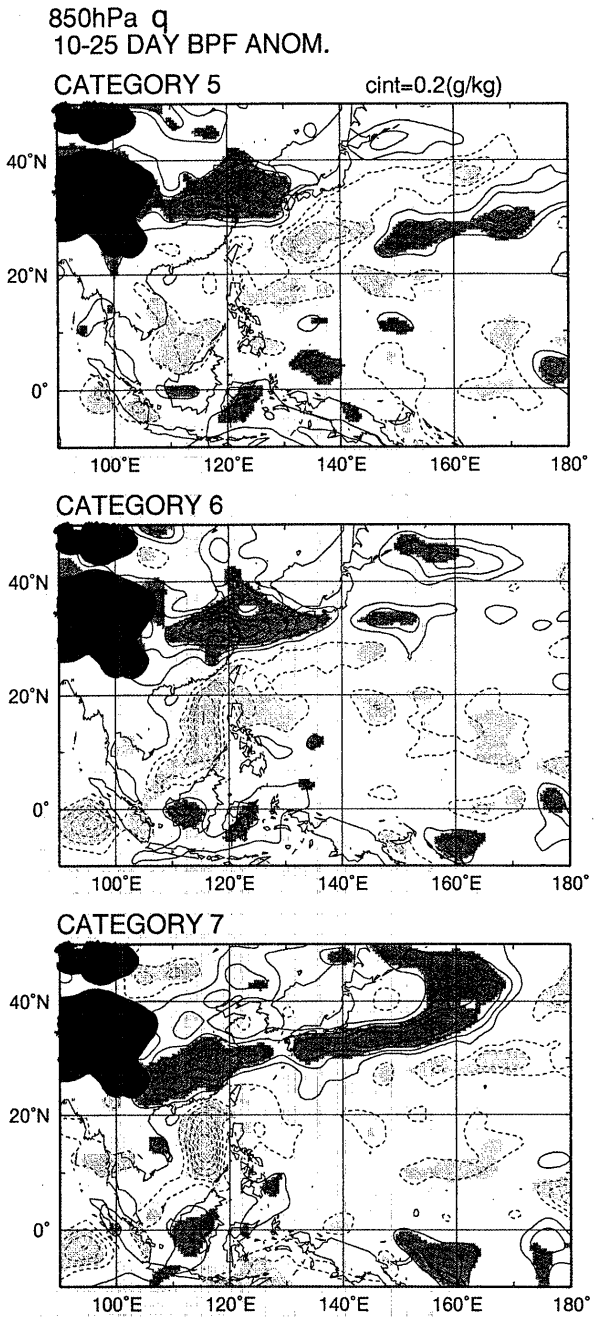

Fig. 9. As in Fig. 8 except for specific humidity anomalies. Contour interval is 0.2 $g\ kg^{-1}$ and locally statistically significant regions are shaded.

level circulation along the coast of East Asia as part of the dynamical interactions between the tropics and the extratropics.

5.3 Circulation anomalies in the upper troposphere

Variations in upper-level circulation associated with 10–25-day convective activity in the South China Sea region are also examined. Composite anomalies of OLR and 200-hPa wind for Category 2 through 4 are presented in Fig. 10 to show the circulation features before and after the stage of peak convection. In Category 2, which is just before the convective peak, a downstream wave train from China into the North Pacific has already emerged. In Category 3, which is the convective peak, divergence pattern is most intensified with the center of divergence near the convective maximum, which is obviously associated with upward motion

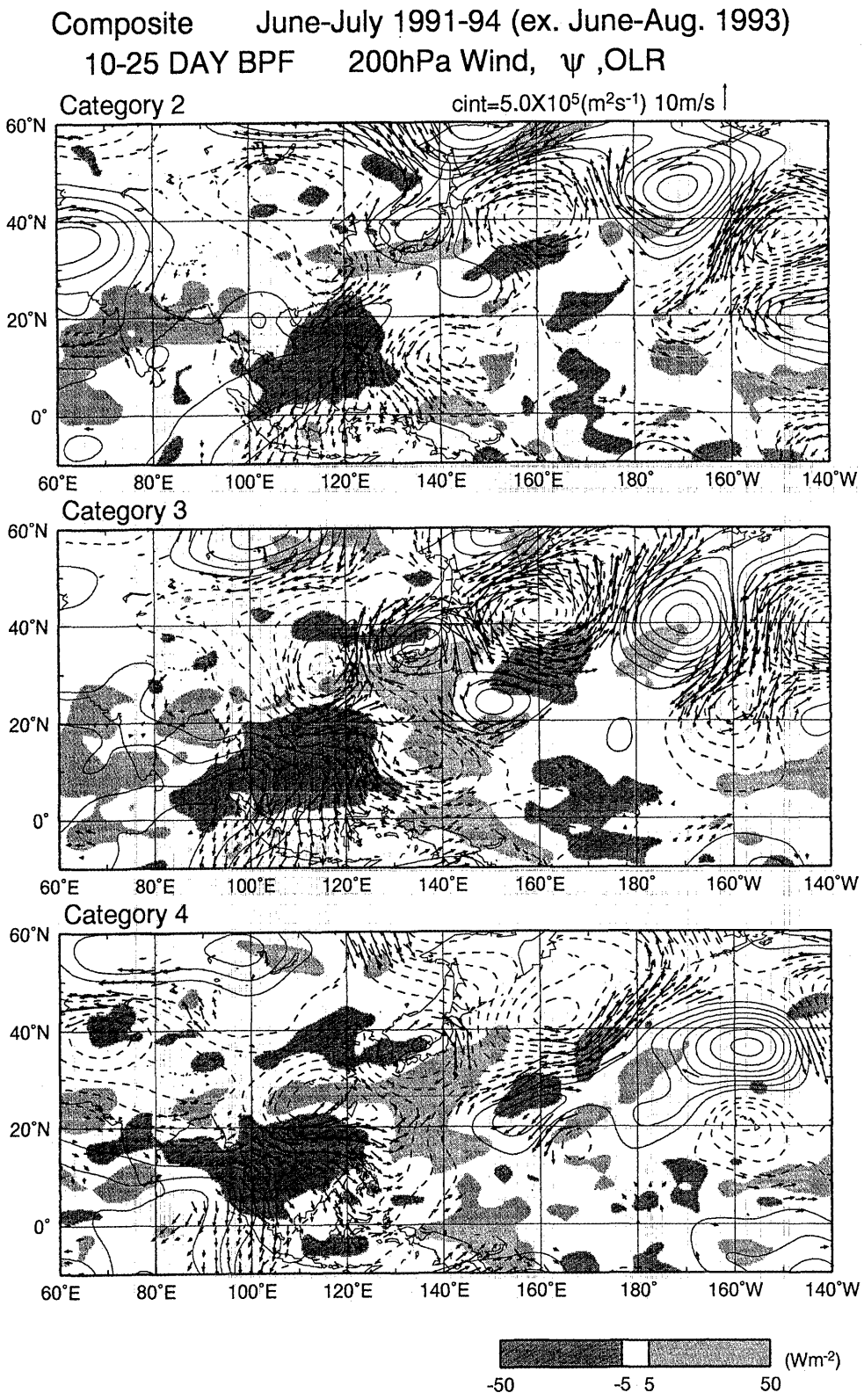

Fig. 10. As in Fig. 7, but for 200-hPa circulation from Category 2 through 4. Contour interval is 5.0×10^5 m^2 s^{-1}.

due to anomalous heating. Cross-equatorial outflow (northerly) is apparent over the maritime continent. An anti-cyclonic pattern in contrast to the low-level cyclonic circulation implies a baroclinic vertical structure of the disturbance over the heating. A well-developed downstream wave train arching into the North Pacific, which is probably forced as a train of Rossby waves can be seen. A cyclonic circulation accompanied by westerly and southwesterly divergent flow is located to the north of divergent center at about 30°N. One can also observe that poleward wind anomalies blow toward an anti-cyclonic circulation over Japan. The location of this anti-cyclonic circulation is almost consistent with that at 850-hPa level (Fig. 8). Following the convective peak (Category 4), the mid-latitude wave train decays slightly. Westerly anomalies to the north of the divergent center progress westward along 15°N–20°N.

In Category 7 (not shown) the circulation pattern is reverse as compared to Category 3. The center of convergent inflow exists over the South China Sea in contrast to Category 3. As seen before, anomalous convection at this stage is extremely suppressed. Downward motion that dominates this stage suggests that periodical changes of the local Hadley circulation occur as shown by Chen and Chen (1995). There is a wave train extending to the North Pacific, which is probably excited by anomalous cooling over the South China Sea region.

In short, systematic changes due to 10–25-day convective activity in the South China Sea region are found also in upper-level circulation over a broad region from Southeast Asia through the North Pacific. The divergent outflow occurs in response to anomalous heating. A downstream wave train in the mid-latitude and westward propagating wind anomalies along the off equatorial tropics is clearly shown. Ambrizzi *et al.* (1995) detected the upper-level waveguide for 10–30-day waves in the Asian and Pacific westerly jet during the JJA season. The location of the wave train in Fig. 11 is in good agreement with their results. Moreover, the present connections between tropical convection and upper-level wave train roughly resemble to those between the sub-monthly (6–30 days) scale tropical convection, and forced upper level waves provided by Kiladis and Weickmann (1992), Schrage and Vincent (1996), and Meehl *et al.* (1996). Though Kiladis and Weickmann (1997) also investigated convection on the sub-monthly time scale over the South China Sea and associated circulation during the JJA season, significant wave train dose not seem to appear in their results. However, our present results suggest that convection in the 10–25-day range over the South China Sea is one of the key factors for the generation of upper-level waves on this time scale, over a broad Asian and Pacific region during the early summer season.

Before the end of this subsection, we provide the barotropic component of stream function anomalies at Category 3 in order to stress the existence of Rossby wave emanation on this time scale. The barotropic component is decomposed from the 850- and 200-hPa value of stream function anomalies $\hat{\psi}$, which is expressed by $(\hat{\psi}_{200}+\hat{\psi}_{850})/2$. A significant wave train emanating from southern China through the eastern North-Pacific is seen in Fig. 11. This wave train is almost arching along a great circle route connecting 22.5°N, 115°E and 40°N, 140°E. This feature indicates that monsoon convection on this time scale can generate a barotropic Rossby wave train from the WNPM region to the mid-latitudes.

6. Summary and discussion

In this paper, some features of large-scale circulation associated with regional convective events occurring in the 10–25-day range during the early summer season were investigated. It is found that the quasi-periodic oscillation of convection in the South China Sea region is closely connected to the circulation and convection in the whole Asia-Pacific region. In addition, the tropical-extratropical linkage in the large-scale circulation systems excited by this convection is identified. These characteristics are summarized and discussed in the present section.

High amplitude OLR fluctuation on the 10–25-day timescale is prominent over the South China Sea. The fluctuation of this time scale explains more than 30 percent of total variance during the early summer season. The maximum OLR variability on this time scale is located over the South China Sea during the early summer season.

Results of the composite analysis indicate that well-defined convective disturbance develops over the South China Sea in the lower level. Enhanced (suppressed) convection is associated with a cyclonic (anti-cyclonic) circulation at 850-hPa level. These disturbances are also associated with zonal wind variation along the off equatorial tropics along 5°–15°N. These tropical westerly (easterly) anomalies propagate westward from east of Philippines to the Arabian Sea, which causes increasing (decreasing) signals of the monsoon westerly flow. This propagating nature is in contrast to that of the MJO time scale variation. As has been shown in many of previous studies, zonal wind anomalies associated with the MJO progress eastward from the Arabian Sea and penetrate to the western Pacific along the position of mean monsoon westerlies.

This convective activity over the South China Sea is closely connected to the circulation and convection in the BFZ region. An anti-cyclonic circulation located at the subtropics near Japan turns up as part of a downstream wave train arching into the North Pacific following the convective peak. Local

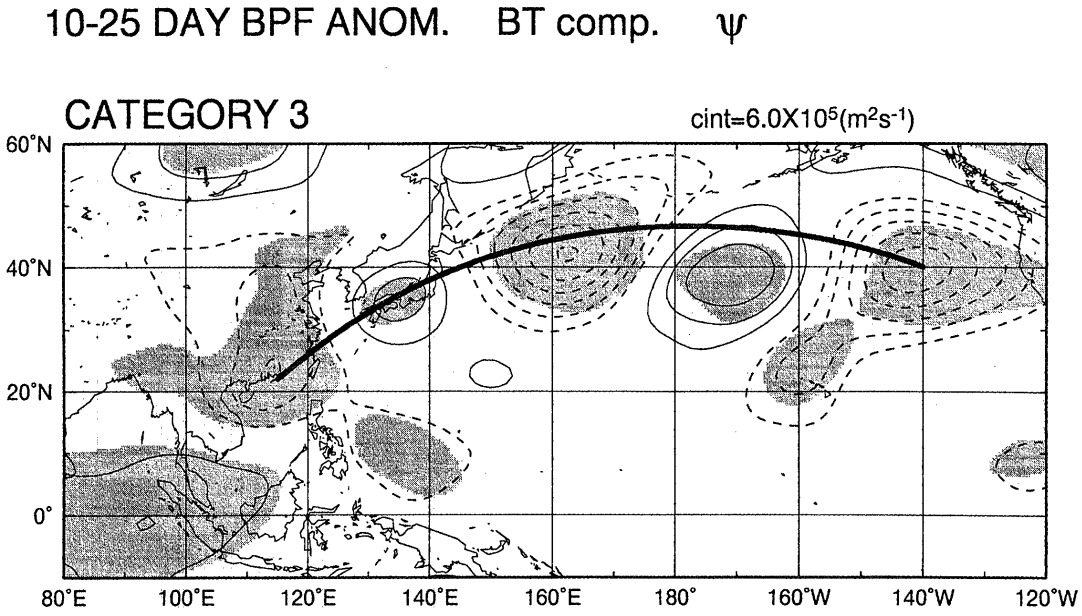

Fig. 11. Barotropic component of stream function anomalies at Category 3. Contour interval is 6.0×10^5 m^2 s^{-1}. Locally statistically significant reions are shaded. A bold line indicates the great circle route.

westerlies at the northern flank of this anti-cyclonic cell play a role to accelerate the low-level subtropical westerlies near the East China Sea and Japan. In addition, the anomalous convection is coupled with these wind anomalies and its coverage area forms a zonally elongated band in the subtropics. The intensification of this subtropical convection is attributed to the increase of moisture transport associated with the maintenance of this local anti-cyclonic circulation. For better understanding the simultaneous relationships between the 10–25-day convection over the South China Sea and that in the subtropics, composite maps of the total stream function at 850 hPa and OLR less than 220 W m^{-2} for the active and inactive phases of the convection over the South China Sea are illustrated in Fig. 12. At the active phase (Category 3), the monsoon trough deepens and extends to the convective maximum over the South China Sea region. At the same time, there is little convective activity with OLR less than 220 W m^{-2} in the subtropics. At the inactive phase (Category 7), the convective activity and trough weakens over the South China Sea and the subtropical ridge over the western North-Pacific seems to be more tight than the active phase. On the other hand, the development of zonally elongated zone of low OLR less than 220 W m^{-2} is evident in the BFZ region. This feature indicates a substantial increase of subtropical convection at this stage.

Furthermore, in upper-level circulation, divergence (convergence) patterns are prominent at the peak of enhanced (suppressed) convection over the South China Sea, which implies that a periodical change of the local Hadley circulation arises from this convective activity. An upper-level wave train emerges in the mid-latitude in response to this tropical convection. These features suggest that this quasi-periodic convective activity is an effective forcing for the upper-level circulation.

It is worth noting that the tropical-extratropical linkage is remarkable on the 10–25-day timescale in the lower level. A significant wave train is formed in Category 3 to 4 (7 to 8). As a basic state, mean westerlies are located continuously from the tropical monsoon region to the North Pacific in this season. These mean basic westerlies probably act as a wave duct, which create a favorable condition for Rossby wave propagation induced by local convective heating (cooling) on this time scale. This situation resembles the wave propagation from WNPM region to the North Pacific on longer timescales (*e.g.*, Tsuyuki and Kurihara, 1989; Kawamura *et al.*, 1996). It is reasonable to suppose that the same mechanism can also be applied to the present results.

In addition, an anti-cyclonic (cyclonic) circulation is built up near Japan as part of a downstream wave train. These subtropical cells maintain their strength and move southwestward into the South China Sea region. The maintenance of these cells is likely to be caused by the interaction between 10–25-day transients and time-mean flow. Further dynamical analysis on the maintenance of 10–25-day wave is required to support this hypothesis. Southwestward retrograding anti-cyclonic (cyclonic) circulation appears to be trapped by the tropical monsoon westerlies, and trigger the suppressed (enhanced) convection over the South China Sea. At the same time

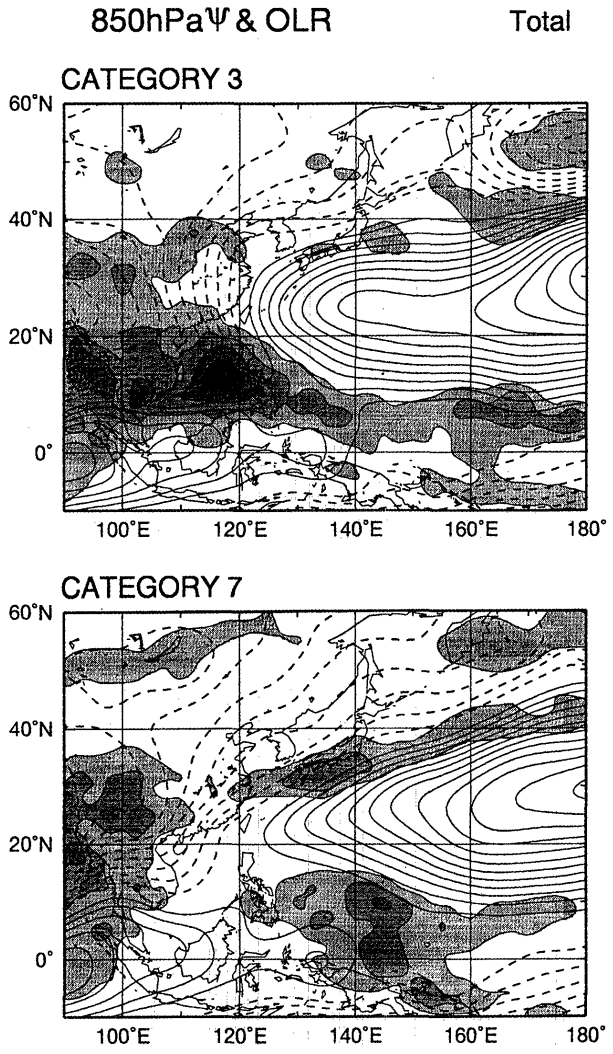

Fig. 12. Total stream function at 850 hPa and OLR less than 220 W m^{-2} for Category 3 and 7. The contour interval is 10×10^5 m^2 s^{-1}, and 20 W m^{-2}. OLR contour and shading indicate regions of OLR less than 220 W m^{-2}.

the suppressed (enhanced) convection seems to force the anti-cyclonic (cyclonic) circulation. The mutual interaction between this southwestward moving cell and convection, as a two-way interaction between the tropics and the subtropics may contribute to the development of disturbance over this region.

The dynamics of the amplification of convective disturbance over the South China Sea is one of the remarkable aspects to be explored. The composite horizontal structure of disturbance in the lower level at the convective peak (Fig. 7) seems to resemble that of the asymmetric equatorial Rossby mode simulated by Xie and Wang (1996). Xie and Wang (1996) and Wang and Xie (1997) discuss the importance of the vertical easterly shear of the mean zonal flow and the surface friction-induced moisture convergence in the mean moist unstable condition for development of unstable disturbance over the tropical monsoon region. The mean flow conditions during the present analysis period are similar to the basic state for their model experiment. However, the primary track of circulation anomaly in the WNPM region in Fig. 7 seems to be different from that by Wang and Xie (1997). The northwestward traveling nature of disturbance seen in their study is not prominent in the present case. Detailed observational analyses based upon high-quality data and further comparison with theoretical modeling studies are required to understand the formation of the disturbance on this shorter time scale over the South China Sea.

Overall, we have focused mainly on the observational evidence for the evolution of large-scale circulation systems associated with 10–25-day convection over the South China Sea during the early summer season. Some interesting characteristics are shown on the basis of the composite results although we have examined only four early summer seasons. The composite results have presented a series of evidences of the linkage between the ITCZ in the WNPM region, and the subtropical convergence zone (STCZ) (Kodama, 1993) in the EAM region on this shorter intraseasonal time scale. Further investigation about the modification of the subtropical circulation through the multi-scale tropical-extratropical interaction in this season would be required. We also need to check whether the series of observational results are reproduced in current GCM results or not. Investigation on this shorter intraseasonal mode probably provides useful information to extended-range weather forecasting as described by Ko and Vincent (1995, 1996). Although our present discussions are concentrated primarily on 10–25-day variations, the dynamical relationship between convective disturbance in the 10–25-day range and the MJO time scales should be examined, including the regional interaction between the tropics and the extratropics on these time scales. This aspect will be reported elsewhere.

Acknowledgments

The authors sincerely appreciate Dr. R. Kawamura, Toyama University, for his advice and helpful suggestion. We also acknowledge the valuable comments and suggestions made by the anonymous reviewers that greatly improved the earlier version of the manuscript. Dr. H. L. Tanaka made the ECMWF data were obtained from the NOAA Climate Diagnostics Center (http://www.cdc.noaa.gov). Most pictures were drawn by the Generic Mapping Tools (GMT) (Wessel and Smith 1991). This work was supported in part by Grant-In-aid from the Ministry of Education (No. 07304069).

References

Ambrizzi, T., B.J. Hoskins and H.-H. Hsu, 1995: Rossby wave propagation and teleconnection patterns in the austral winter. *J. Atmos. Sci.*, **52**, 3661–3672.

Chen, T.-C. and M. Murakami, 1988: The 30–50 day variation of convective activity over the Western Pacific Ocean with emphasis on the Northwestern region. *Mon. Wea. Rev.*, **116**, 892–906.

Chen, T.-C. and J.-M. Chen, 1993a: The intraseasonal oscillation of the lower-troposheric circulation over the Western Pacific during the 1979 northern summer. *J. Meteor. Soc. Japan*, **71**, 205–220.

Chen, T.-C. and J.-M. Chen, 1993b: The 10–20-day mode of the 1979 indian monsoon: Its relation with the time variation of monsoon rainfall. *Mon. Wea. Rev.*, **121**, 2465–2482.

Chen, T.-C. and J.-M. Chen, 1995: An observational study of the South China Sea monsoon during the 1979 summer: Onset and life cycle. *Mon. Wea. Rev.*, **123**, 2295–2318.

Gilman, D.L., F.J. Fuglister and J.M. Mitchell Jr., 1963: On the power spectrum of "Red Noise." *J. Atmos. Sci.*, **20**, 182–184.

Hsu, H.-H. and S.-H. Lin, 1992: Global teleconnections in the 250-mb streamfunction field during the Northern Hemisphere winter. *Mon. Wea. Rev.*, **120**, 1169–1181.

Kato, K., 1989: Seasonal transition of the low-level Circulation systems around the Baiu front in China in 1979 and its relation to the northern summer monsoon. *J. Meteor. Soc. Japan*, **67**, 249–265.

Kawamura, R, T. Murakami and B. Wang, 1996: Tropical and mid-latitude 45-day perturbations over the western Pacific during the northern summer. *J. Meteor. Soc. Japan*, **74**, 867–890.

Kaylor, R.E., 1977: Filtering and decimation of digital time series. *Tech. Note BN 850*, Institute of Physical Science Technology, University of Maryland, College Park, 42pp.

Kiladis, G.N. and K.M. Weickmann, 1992: Circulation anomalies associated with tropical convection during northern winter. *Mon. Wea. Rev.*, **120**, 1900–1923.

Kiladis, G.N. and K.M. Weickmann, 1997: Horizontal structure and seasonality of large-scale circulations associated with submonthly tropical convection. *Mon. Wea. Rev.*, **125**, 1997–2013.

Ko, K.-C. and D.G. Vincent, 1995: A composite study of the quasi-periodic subtropical wind maxima over the South Pacific during November 1984-April 1985. *J. Climate*, **8**, 579–588.

Ko, K.-C. and D.G. Vincent, 1996: Behavior of one to two week summertime subtropical wind maxima over the South Pacific during ENSO cycle. *J. Climate*, **9**, 5–16.

Kodama, Y.-M., 1992: Large-scale common features of subtropical precipitation zones (the Baiu frontal zone, the SPCZ, and the SACZ) Part I: Characteristics of subtropical frontal zones. *J. Meteor. Soc. Japan*, **70**, 813–836.

Kodama, Y.-M., 1993: Large-scale common features of subtropical precipitation zones (the Baiu frontal zone, the SPCZ, and the SACZ) Part II: Conditions of the circulations of generating the STCZs. *J. Meteor. Soc. Japan*, **71**, 581–610.

Kodama, Y.-M., 1997: Airmass transformation of the Yamase air-flow in the summer of 1993. *J. Meteor. Soc. Japan*, **75**, 737–751.

Krishnamurti, T.N. and H.N. Bhalme, 1976: Oscillations of a monsoon system. Part I: Observational aspects. *J. Atmos. Sci.*, **33**, 1937–1954.

Krishnamurti, T.N. and P. Ardanuy, 1980: The 10-to-20-day westward propagating mode and "breaks in the monsoons." *Tellus*, **32**, 15–26.

Krishnamurti, T.N. and D. Subrahmanyam, 1982: The 30–50 day mode at 850 mb during MONEX. *J. Atmos. Sci.*, **39**, 2088–2095.

Lau, K.-M. and P.H. Chan, 1986: Aspecs of the 40–50 day oscillation during the northern summer as inferred from outgoing longwave radiation. *Mon. Wea. Rev.*, **114**, 1354–1367.

Lau, K.-M., G.J. Yang and S.H. Shen, 1988: Seasonal and intraseasonal climatology of summer monsoon rainfall over East Asia. *Mon. Wea. Rev.*, **116**, 18–37.

Lau, K.-M., 1992: East Asian summer monsoon rainfall variability and climate teleconnection. *J. Meteor. Soc. Japan*, **70**, 211–242.

Lau, K.-M. and S. Yang, 1996: Seasonal variation, abrupt transition, and intraseasonal variability associated with the Asian summer monsoon in the GLA GCM. *J. Climate*, **9**, 965–985.

Madden, R.A. and P.R. Julian, 1971: Detection of a 40-50 day oscillation in the zonal wind in the tropical Pacific. *J. Atmos. Sci.*, **28**, 702–708.

Madden, R.A. and P.R. Julian, 1972: Description of global scale circulation cells in the tropics with a 40–50 day period. *J. Atmos. Sci.*, **29**, 1109–1123.

Meehl, G.A., G.N. Kiladis, K.M. Weickmann, M. Wheeler, D.S. Gutzler and G.P. Compo, 1996: Modulation of equatorial subseasonal convective episodes by tropical-extratropical interaction in the Indian and Pacific Ocean regions. *J. Geophys. Res.*, **101**, 15033–15049.

Mitchell, J.M., Jr., 1966: Climate Change. *Tech. Note 79*, World Meteorological Organization, 36–42.

Murakami, M., 1976: Analysis of summer monsoon fluctuations over India. *J. Meteor. Soc. Japan*, **54**, 15–32.

Murakami, T., T. Nakazawa and J. He, 1984a: On the 40–50 day oscillation during the 1979 Northern Hemisphere summer. Part I: Phase propagation. *J. Meteor. Soc. Japan*, **62**, 440–468.

Murakami, T., T. Nakazawa and J. He, 1984b: On the 40–50 day oscillation during the 1979 Northern Hemisphere summer. Part II: Heat and moisture budget. *J. Meteor. Soc. Japan*, **62**, 469–484.

Murakami, T. and J. Matsumoto, 1994: Summer monsoon over the Asian continent and Western Pacific. *J. Meteor. Soc. Japan*, **72**, 719–745.

Murakami, T., 1987: Intraseasonal atmospheric teleconnection patterns during the Northern Hemisphere summer. *Mon. Wea. Rev.*, **115**, 2133–2154.

Nakazawa, T., 1986: Intraseasonal variations of OLR in the tropics during FGGE year. *J. Meteor. Soc. Japan*, **64**, 17–34.

Ninomiya, K. and H. Muraki, 1986: Large-scale circulations over East Asia during the Baiu period of 1979. *J. Meteor. Soc. Japan*, **64**, 409–429.
Ninomiya, K. and T. Akiyama, 1992: Multi-scale features of Baiu, the summer monsoon over Japan and the East Asia. *J. Meteor. Soc. Japan*, **70**, 467–495.
Schrage, J.M. and D.G. Vincent, 1996: Tropical convection on 7–21 day timescales over the Western Pacific. *J. Climate*, **9**, 587–607.
Tsuyuki, T. and K. Kurihara, 1989: Impact of convective activity in the western tropical Pacific on the East Asian summer circulation. *J. Meteor. Soc. Japan*, **67**, 231–247.
Wang, B. and X. Xie, 1997: A model for the boreal summer intraseasonal oscillation. *J. Atmos. Sci.*, **54**, 72–86.
Wessel, P. and W.H.F. Smith, 1991: Free software helps map and display data. *EOS Trans. AGU*, **72**, 441, 445–446.
Xie, X. and B. Wang, 1996: Low-frequency equatorial waves in vertically sheared zonal flow. PartII: Unstable waves. *J. Atmos. Sci.*, **53**, 3589–3605.
Yasunari, T., 1979: Cloudiness fluctuations associated with the Northern Hemisphere summer monsoon. *J. Meteor. Soc. Japan*, **57**, 227–242.
Yasunari, T., 1981: Structure of an Indian summer monsoon system with around 40-day period. *J. Meteor. Soc. Japan*, **59**, 336–354.

初夏の東アジアおよび西部北太平洋域にみられる対流活動と循環場の10–25日季節内変動

福富慶樹
（筑波大学地球科学研究科）
安成哲三
（筑波大学地球科学系）

1991–94年初夏の東アジアおよび西部北太平洋モンスーン域における対流活動と循環場の10–25日周期季節内変動についてデータ解析を行った。特に、同時間スケールで変動する南シナ海上の対流活動と東アジア亜熱帯域の下層循環場の関係に注目し、コンポジット解析を適用して調べた結果、この対流活動がアジア–太平洋域の大規模循環場の変動に関係しており、これを通じて亜熱帯域の循環場の発達をもたらす側面が明らかになった。

南シナ海上の10–25日スケールの対流活動は、その活発(不活発)時には下層の低気圧(高気圧)性循環偏差を伴っている。それらのピーク時には南シナ海付近から北太平洋に向かって波列が形成され、これは加熱(冷却)偏差に対するRossby応答であると考えられる。南シナ海上の対流活動の活発のピークに引き続いてこの波列の一部分として東アジア亜熱帯域に発生する高気圧性偏差は、それに沿った下層水蒸気輸送を強化し、その北縁の亜熱帯対流活動の強化に寄与することができる。同時にこの高気圧性偏差は南シナ海に向かって南西進し、南シナ海上の次の対流活動の抑制を引き起こしている。逆に南シナ海上の不活発時に引き続いて亜熱帯域から南西進する低気圧性偏差は、次の南シナ海上の対流活動の活発化をもたらす。これらの特徴は、同時間スケールの熱帯–亜熱帯間の相互作用が、同領域のモンスーン循環の変動にとって重要な役割を果たす事を示している。

対流圏上層においては、同時間スケールの対流活動の活発(不活発)時に南シナ海上で強い発散(収束)場が発生すると同時に中緯度偏西風帯の波列構造が最も強化されており、この対流活動が広領域の上層循環場へ作用していることを示唆する。以上の事により、南シナ海上の10–25日周期の対流活動は、初夏の大規模循環場に対する効果的な強制としての役割を果たすことが確認された。